Article

Discovery Medicine 2026; 38(211): 2406–2417
https://doi.org/10.24976/Discov.Med.202638211.190

Patchouli Alcohol: A Natural Cardioprotectant Against Adriamycin-Induced Heart Failure

Shumin Lv[1], Hongwen Cai[1], Zhijun Wang[1], Jianhua Ye[2], Ligang Bao[2,*]

[1]Department of Cardiology, The First Affiliated Hospital of Zhejiang Chinese Medical University (Zhejiang Provincial Hospital of Chinese Medicine), 310006 Hangzhou, Zhejiang, China
[2]Department of Cardiology, Tongde Hospital of Zhejiang Province, 310012 Hangzhou, Zhejiang, China
*Correspondence: baoligang2011@163.com (Ligang Bao)
Submitted: 26 March 2026 Revised: 21 April 2026 Accepted: 12 May 2026 Published: 24 August 2026

Background: Patchouli alcohol (PA), a tricyclic sesquiterpene from *Pogostemonis Herba*, exhibits anti-inflammatory, antioxidant and cardiovascular activities. Adriamycin (Adr) induces dose-dependent cardiotoxicity that progresses to irreversible heart failure (HF). This study investigated the mechanism of PA in rats with Adr-induced HF.
Methods: Male Sprague Dawley (SD) rats (initial n = 15/group) received intraperitoneal Adr (2 mg/kg, twice weekly for 4 weeks) to induce HF. Two weeks after modeling, PA (30 mg/kg/d) or Icilin (20 mg/kg/d) was administered for 4 weeks. Cardiac function (left ventricular ejection fraction (LVEF)/left ventricular short axis shortening rate (LVFS)), serum brain natriuretic peptide (BNP), lactate dehydrogenase (LDH), creatine kinase (CK), nitric oxide (NO), nitric oxide synthase (NOS), aspartate aminotransferase (AST), myocardial transient receptor potential melastatin 8 (TRPM8) and apoptosis-related proteins (Bcl-2 associated X protein (Bax), B-cell Lymphoma 2 (Bcl-2), and cleaved Caspase-3) were assessed. *In vitro*, Adr-treated AC16 cells were used to confirm the anti-apoptotic role of TRPM8 through PA treatment, N-(4-tert-butylphenyl)-N′-(3-chloro-4-fluorophenyl)urea (BCTC), and TRPM8 manipulation.
Results: *In vivo*, PA and Icilin ameliorated cardiac dysfunction in Adr-induced HF rats ($p < 0.05$), downregulated HF markers and myocardial injury factors ($p < 0.05$), and mitigated Adr-induced myocardial pathological damage. Both agents also upregulated myocardial TRPM8 expression ($p < 0.001$) and reversed Adr-induced abnormal apoptosis-related proteins ($p < 0.05$), thus inhibiting excessive cardiomyocyte apoptosis. *In vitro*, PA suppressed Adr-induced AC16 cardiomyocyte apoptosis by upregulating TRPM8 ($p < 0.01$), whereas TRPM8 knockdown or inhibition abrogated PA's protective effect ($p < 0.001$).
Conclusion: This study identifies PA as a novel pharmacological enhancer of TRPM8, demonstrating that PA exerts significant cardioprotective effects in Adr-induced HF by targeting TRPM8 and inhibiting cardiomyocyte apoptosis. These findings support TRPM8 as a key mediator of PA's protective role and provide a promising therapeutic strategy for HF management.

Keywords: patchouli alcohol; heart failure; adriamycin; TRPM8; apoptosis

Introduction

Heart failure (HF) is the end-stage manifestation of various cardiovascular diseases, characterized by high morbidity and mortality [1,2]. Adriamycin (Adr), an anthracycline chemotherapeutic agent, is widely used to establish HF animal models due to its dose-dependent cardiotoxicity and high affinity for cardiac tissue [3–6]. Adr-induced cardiomyopathy and congestive HF closely recapitulate clinical anthracycline cardiotoxicity, with myocardial remodeling as a key underlying mechanism [7]. However, effective cardioprotective agents against Adr-induced HF remain limited, underscoring the need for novel therapeutic interventions.

In recent years, the advantages of traditional Chinese medicine (TCM) in the treatment of HF have gradually emerged [8]. *Pogostemonis Herba* is a TCM in China, and Chinese patent medicine preparations containing *Pogostemonis Herba* as the main ingredient are increasingly available [9]. As a major component of the volatile oil of *Pogostemonis Herba*, patchouli alcohol (PA) is a naturally derived tricyclic sesquiterpene with anti-inflammatory, antiviral, antioxidant, antibacterial, neuroprotective, anticancer, and gastrointestinal regulatory activities [10]. Some studies have confirmed that PA can regulate the activities of various cardiac hypertrophy-related cytokines including nitric oxide and aspartate aminotransferase (AST) [11,12]. Analysis using the SwissTargetPrediction database indicated that PA may modulate transient receptor potential melastatin 8 (TRPM8). Activation of TRPM8 has been reported to attenuate inflammation and cardiac remodeling after myocardial infarction [13]. However, whether PA can ameliorate Adr-induced HF in rats by modulating TRPM8 expression has yet to be reported.

In this study, Adr was used to establish a rat model of HF. We aimed to investigate the effects and underlying

mechanisms of PA and the TRPM8 activator icilin on myocardial histopathology in Adr-induced HF rats.

Materials and Methods

Ethics Statement

All experimental procedures were approved by the Committee of Laboratory Animals of Zhejiang Provincial Animal Center (ZJCLA-IACUC-20120022) and performed in accordance with the regulations of the China Animal Care and Use Committee. All efforts were made to minimize animal suffering.

Preparation of HF Model in Rats

In this study, a total of 60 specific pathogen free (SPF) male Sprague Dawley (SD) rats (200 ± 20 g) were acquired from Beijing Vital River Laboratory Animal Technology Co., Ltd. Animal license number: SCXK (Beijing) 2019-0301. All animal experiments were conducted in the SPF laboratory animal center. Room temperature was maintained at 22–25 °C, relative humidity was controlled at 45%–65%, and SD rats were acclimatized under standard feeding conditions for 5 days before the experiment.

The HF model was established as previously described [14]. Adriamycin (Adr, D1515, Sigma-Aldrich, St. Louis, MO, USA) was dissolved in 0.9% normal saline (B020, Nanjing Jiancheng Bioengineering Institute, Nanjing, China) to prepare a 0.8 mg/mL solution, and then SD rats were intraperitoneally injected with Adr at 2 mg/kg twice weekly for 4 weeks. The cumulative dose of each SD rat was 16 mg/kg. Rats in the normal control group were intraperitoneally injected with anequal volume of normal saline. Two weeks after the last Adr injection, symptoms including dyspnea, depilation, poor mental state, ascites, and decreased rectal temperaturewere observed, indicating successful establishment of the HF model.

Animal Grouping and Drug Treatment

A total of 60 male SD rats were randomly allocated to 4 groups (n = 15 per group initially): blank group, Adr group, Adr + PA group, and Adr + TRPM8 activator (Icilin) group. Sample size was determined based on power analysis (effect size = 0.8, $\alpha = 0.05$, power = 0.8), which estimated a minimum of 12 rats per group; we included 15 rats per group to account for potential mortality during the 10-week experimental period. Final sample sizes after mortality were: blank group, n = 15; Adr group, n = 12; Adr + PA group, n = 14; Adr + Icilin group, n = 13. In the Adr + PA group, 2 weeks after the modeling, PA (05690595, Sigma-Aldrich, St. Louis, Missouri, USA) was dissolved in 2% Tween 80 in saline and intraperitoneally administered at 30 mg/kg/d for 4 weeks [15]. In the Adr + Icilin group, 2 weeks after the modeling, icilin (Cat. No. 1531/10, Tocris bioscience, Bristol, England, UK) was prepared in 2% Tween 80 in saline and intraperitoneally administered at 20 mg/kg/d for 4 weeks. This icilin dose was selected based on a previous study showing that intraperitoneal injection of icilin at 20 mg/kg effectively activates TRPM8 channels *in vivo* [16], as well as our preliminary dose-finding experiments. In each group of 12 mice, six mice were used for serum BNP measurement and myocardial H&E staining, while the other six were used for serum AST/LDH/CK measurement and myocardial Western blotting.

Preparation of Serum Samples and Myocardial Tissue Samples

After treatment, SD rats were anesthetized with pentobarbital sodium at a dose of 40 mg/kg (283256, Shanghai Xinyu Biotechnology Co., Ltd., Shanghai, China). The heart was then exposed and blood was collected from the right ventricle using a disposable vacuum blood collection needle. Next, the collected serum was centrifuged at 4 °C, 3000 revolutions per minute (rpm) for 15 minutes (min), and the supernatant was aspirated and kept at –80 °C.

After blood collection, SD rats were euthanized by cervical dislocation. Then, the heart tissues were immediately excised and placed in pre-cooled physiological saline to remove residual blood. The tissues were blotted dry with absorbent paper, and a portion of the myocardial tissues was transferred to a high-throughput tissue grinder (E1644, Beyotime, Shanghai, China), ground at a frequency of 9.5 Hertz (Hz) for 20 min, and then centrifuged at 4 °C, 12,000 rpm for 10 min to collect the supernatant. The remaining myocardial tissues were stored at –80 °C and used for quantitative real-time polymerase chain reaction (qRT-PCR), western blotting, and Hematoxylin and Eosin (H&E) staining.

Enzyme-Linked Immunosorbent Assay (ELISA)

The brain natriuretic peptide (BNP) kit (BPE30445), lactate dehydrogenase (LDH) kit (BPE30024), creatine kinase (CK) kit (BPE30279), and AST kit (BPE20184) were purchased from Lengton (Shanghai, China), and the nitric oxide (NO) kit (E-BC-K035-M) was purchased from Elabscience (Houston, Texas, USA). Next, the prepared serum or myocardial tissue supernatants were diluted as needed and added to the 96-well plates along with anti-BNP/LDH/CK/AST/NO antibody and streptavidin-HRP, then incubated at 37 °C for 60 min. Subsequently, color-developing agents A and B were added to each well, and the plate was incubated at 37 °C for 10 min in the dark. Afterward, stop solution was added. The absorbance (450 nm) was estimated by a microplate reader (PLUS 384, Molecular Devices, San Jose, California, USA).

Detection of Nitric Oxide Synthase (NOS)

The NOS kit (S0025) was purchased from Beyotime (Shanghai, China). Myocardial tissue supernatants were added to 100 µL NOS detection buffer, followed by 100 µL of detection reaction solution. The myocardial tissue su-

Table 1. Gene sequence primers.

Name	Forward primer (5′-3′)	Reverse primer (5′-3′)
ANP/NPPA	CACAGATCTGATGGATTTCAAGA	CCTCATCTTCTACCGGCATC
BNP/NPPB	AGAACAATCCACGATGCAGA	CCTTGGTCCTTTGAGAGCTG
Caspase-3	TCCACGAGCAGAGTCAAAGG	AACAAGCCAACCAAGTTCACA
Bax	AATATGGAGCTGCAGAGGATGA	CCCCCATTCATCCCAGGAAAA
Bcl-2	TCGCCCTGTGGATGACTGA	CAGAGACAGCCAGGAGAAATCA
TRPM8	CGGTCATCTACGAGCCCTAC	CACACACAGTGGCTTGGACT
β-actin	TGACAGGATGCAGAAGGAGA	TAGAG CCACCAATCCACACA

ANP, atrial natriuretic peptide; NPPA, natriuretic peptide A; BNP, brain natriuretic peptide; NPPB, natriuretic peptide B; Bcl-2, B-cell Lymphoma 2; Bax, Bcl-2 associated X protein; TRPM8, transient receptor potential melastatin 8.

pernatants were then incubated at 37 °C for 20–60 min. Finally, the absorbance of the samples at the excitation wavelength of 495 nm and the emission wavelength of 515 nm was detected by the microplate reader (PLUS 384, Molecular Devices, San Jose, California, USA).

QRT-PCR

Total RNAs from myocardial tissues and AC16 cells were isolated by a Trizol reagent (R0016, Beyotime, Shanghai, China). Next, the BeyoRT™ II cDNA First Strand Synthesis Kit (D7168S, Beyotime, Shanghai, China) was used to synthesize cDNA according to the kit instructions, with total RNA as the template, and the synthesized cDNA was stored at –20 °C until use. Then, qRT-PCR was performed using BeyoFast™ Probe qPCR Mix (D7271, Beyotime, Shanghai, China) on a PCR instrument (CFX96, Bio-Rad, Hercules, California, USA), according to the established reaction system and standard amplification procedure (pre-denaturation at 95 °C for 2 min, 40 cycles of denaturation at 95 °C for 10 s and annealing extension at 60 °C for 30 s). All primers sequences are listed in Table 1. Primer specificity was validated by melting curve analysis (single-peak confirmation) and by 2% agarose gel electrophoresis (single band at the expected size). For each primer pair, amplification efficiency was determined from a standard curve generated by five-fold serial dilutions of cDNA, and calculated as E (%) = (10^(-1/slope)-1)×100. All primer pairs exhibited amplification efficiencies between 90% and 110%, with R^2 values >0.98. A no-template control (NTC) was included in each run to exclude primer-dimer formation or contamination. The mRNA expression levels of target genes were normalized to β-actin, which has been previously validated as a stable reference gene in rat myocardial tissue under pathological conditions [17,18]. Relative quantification was performed using the $2^{-\Delta\Delta Ct}$ method [19].

Western Blot Assay

The treated myocardial tissues and AC16 cells were lysed with RIPA buffer (P0013B, Beyotime, Shanghai, China). Afterward, the BCA kit (P0009, Beyotime, Shanghai, China) was employed to quantify the protein concentration. The proteins were then subjected to electrophoresis and transferred onto PVDF membranes (2215, Millipore, Burlington, MA, USA). Following blocking with 5% non-fat milk at 37 °C for 120 min, the blocked membranes were exposed to anti-atrial natriuretic peptide/natriuretic peptide A (ANP/NPPA, 1:2000, ab180649, 16 kDa, Abcam, Cambridge, UK), anti-BNP/NPPB (1:500, ab19645, 18 kDa, Abcam, Cambridge, UK), TRPM8 (1:1000, PA1-46239, 127 kDa, Thermo Fisher Scientific, Waltham, MA, USA), anti-cleaved Caspase-3 (1:500, ab2302, 17 kDa, Abcam, Cambridge, UK), anti-Caspase-3 (1:500, ab13847, 32 kDa, Abcam, Cambridge, UK), anti-Bax (1:10,000, ab32503, 21 kDa, Abcam, Cambridge, UK), anti-Bcl-2 (1:2000, ab194583, 26 kDa, Abcam, Cambridge, UK) and anti-β-actin (1:3000, ab8227, 42 kDa, Abcam, Cambridge, UK) overnight at 4 °C. Then, the HRP-linked anti-rabbit IgG antibody (1:5000, ab150077, Abcam, Cambridge, UK) was added. Finally, the membranes were incubated with ECL detection reagent (P0018FS, Beyotime, Shanghai, China) and visualized using a gel imager (FluorChem FC3, Alpha Innotech, San Jose, CA, USA). β-actin was used as the normalization control.

Echocardiography

As previously reported [20], the left ventricular ejection fraction (LVEF) and left ventricular short axis shortening rate (LVFS) of SD rats were measured after 4 weeks of treatment. SD rats were anesthetized with pentobarbital sodium at a dose of 40 mg/kg, placed supine on the operating table, and secured to a fixation plate. Next, the ventral chest hair was shaved, and the hearts were scanned with an echocardiograph (Acuson Sequoia model 512, Siemens, Munich, Bavaria, Germany) at a frequency of 25 MHz to measure LVEF and LVFS.

H&E Staining

Myocardial tissues were fixed with 4% paraformaldehyde (P0099, Beyotime, Shanghai, China), dehydrated with graded ethanol, and embedded in paraffin. The paraffin-embedded tissues were cut into 3 µm slices and baked in

a 65 °C oven for 30 min. Next, the slices were dewaxed with xylene, stained with hematoxylin solution (C0107, Beyotime, Shanghai, China) for 5 min, and washed with distilled water for 1 min. Thereafter, the slices were differentiated in 75% hydrochloric acid ethanol for 30 seconds, washed immediately, and blued for 2 min. Subsequently, the slices were stained with 1% eosin solution (C0109, Beyotime, Shanghai, China) for 3 min and dehydrated with graded ethanol. Xylene was used for clearing, and neutral balsam (D054-1-1, Nanjing Jiancheng Bioengineering Institute, Nanjing, China) was used for sealing. Finally, slices were observed under an optical microscope (Ts2R-FL, Nikon, Tokyo, Japan) at 1.2×, 100× and 200× magnification.

Cell Culture

Human myocardial cell line (AC16, MXC1026) was obtained from Meixuan Biotechnology Co., Ltd. (Shanghai, China). AC16 cells were cultured in Roswell Park Memorial Institute-1640 (RPMI-1640) complete medium (M1025, Meixuan Biotechnology Co., Ltd., Shanghai, China), and maintained in a cell incubator (Herocell 180, RADOBIO, Shanghai, China). Cell identity was confirmed by short tandem repeat (STR) profiling, and mycoplasma contamination was confirmed to be negative.

Transfection

A total of 1×10^5 AC16 cells were seeded into 12-well plates and cultured until they reached a confluent monolayer. Small interfering RNA targeting TRPM8 (siTRPM8, abx905813) and its negative control (siNC, abx941273) were obtained from Abbexa (Cambridge, UK). TRPM8 overexpression was achieved by cloning the TRPM8 sequence into the pcDNA3.1 vector (Thermo Fisher Scientific, Waltham, MA, USA). An empty vector was used as the control. The TRPM8 overexpression plasmid and empty vector were transfected into AC16 cells using Lipo6000 (C0526, Beyotime, Shanghai, China).

Cell Treatment

To investigate the roles of PA and TRPM8 in AC16 cells, cells were pretreated with or without 10 μM PA or 3 μM N-(4-tert-butylphenyl)-N′-(3-chloro-4-fluorophenyl)urea (BCTC), a TRPM8 inhibitor (SML0355, Sigma-Aldrich, St. Louis, MO, USA) for 2 h before treatment with 0.5 μM Adr for 24 h. In addition, cells transfected with siNC or siTRPM8 were treated with or without 10 μM PA for 2 h before stimulation with 0.5 μM Adr for 24 h. Cells transfected with the negative control vector or the TRPM8-overexpression plasmid were exposed to 3 μM BCTC for 2 h before stimulating with 0.5 μM Adr for 24 h.

Apoptosis Assessment

Apoptosis in the resulting AC16 cells was evaluated using an Annexin V-FITC/PI kit (C1062L, Beyotime, Shanghai, China). The digested AC16 cells were centrifuged and then re-suspended in 195 μL of 1× binding buffer. After being transferred into centrifuge tubes, each tube was reacted with 5 μL of Annexin V-FITC and 10 μL of PI. Following reaction for 10 min at 37 °C under light-avoidance conditions, apoptosis was analyzed using a PAS III flow cytometer purchased from Partec (Münster, North Rhine-Westphalia, Germany).

Gating and quantitative analysis of apoptosis were performed as follows. After staining, at least 10,000 events were acquired for each sample using a PAS III flow cytometer (Partec, Münster, North Rhine-Westphalia, Germany). Debris and cell doublets were excluded by forward scatter (FSC) versus side scatter (SSC) gating to select the main cell population. Within the selected population, a two-parameter dot plot of Annexin V-FITC (FL1) versus PI (FL3) was generated. Quadrants were set based on the negative control (unstained and single-stained) samples. Cells in the lower-right quadrant (Annexin V^+/PI^-) were defined as early apoptotic cells, those in the upper-right quadrant (Annexin V^+/PI^-) as late apoptotic/necrotic cells, and those in the lower-left quadrant (Annexin V^+/PI^-) as viable cells. The total apoptosis rate was calculated as the sum of early and late apoptotic cells. Data were analyzed using FlowJo software (V.10.0.4, Tree Star, Ashland, OR, USA).

Statistical Analysis

GraphPad Prism 8.0 (GraphPad Software, La Jolla, CA, USA) was used for statistical analysis. Differences among multiple groups were compared using one-way analysis of variance followed by Turkey's post hoc test. Data were expressed as the mean ± standard deviation, and $p < 0.05$ was considered statistically significant.

Results

PA and Icilin Decreased BNP Content, ANP/NPPA and BNP/NPPB Expressions and Improved Cardiac Function in HF Rats

During the experiment, three SD rats died in the Adr group, including one during modeling and two after modeling. One SD rat died in the Adr + PA group during the modeling process. In the Adr + Icilin group, one died in the process of modeling and another died after modeling. To evaluate the effects of PA and Icilin on HF, serum BNP levels were measured by ELISA (Fig. 1A). Adr significantly increased BNP content, whereas PA and Icilin treatment significantly inhibited this increase ($p < 0.05$). Similarly, Adr significantly elevated the mRNA and protein levels of ANP/NPPA and BNP/NPPB in myocardial tissue, and both PA and Icilin reversed these changes (Fig. 1B–D, $p < 0.05$). Cardiac function was assessed by echocardiography. As shown in Fig. 1E,F, Adr markedly reduced LVEF and LVFS, whereas both PA and Icilin significantly

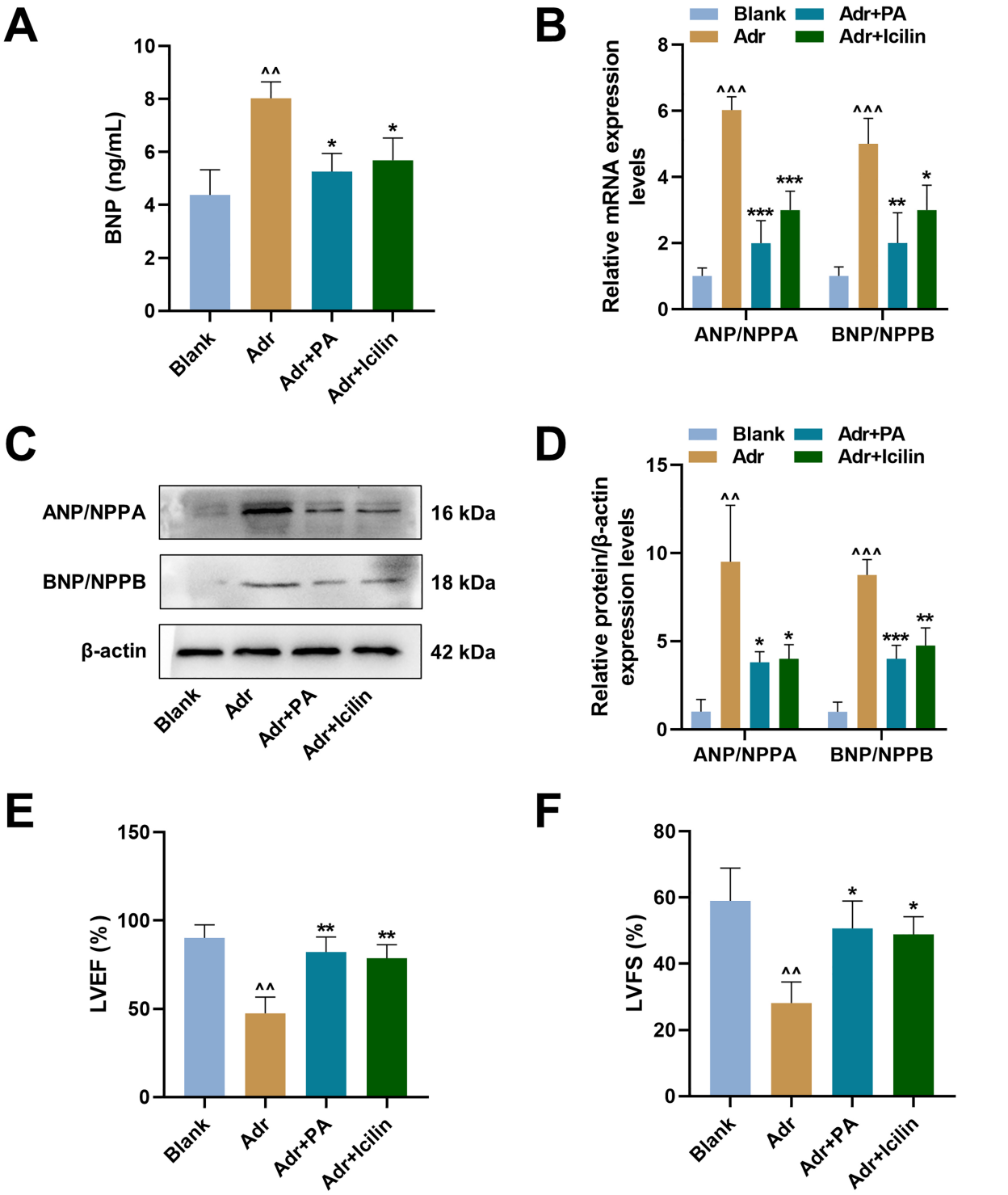

Fig. 1. PA and Icilin decreased BNP content, ANP/NPPA and BNP/NPPB expressions and improved cardiac function in HF rats. (A) The effects of patchouli alcohol (PA) and Icilin (a transient receptor potential melastatin 8 (TRPM8) agonist) on brain natriuretic peptide (BNP) content in adriamycin (Adr)-induced heart failure (HF) rats were detected by enzyme-linked immunosorbent assay (ELISA). (B) Quantitative real-time polymerase chain reaction (qRT-PCR) analysis of atrial natriuretic peptide (ANP)/natriuretic peptide A (NPPA) and BNP/NPPB mRNA levels in myocardial tissues (β-actin as internal control). (C,D) Western blot assay of ANP/NPPA and BNP/NPPB protein expressions in myocardial tissues (β-actin as internal control). (E,F) The left ventricular ejection fraction (LVEF) and left ventricular short axis shortening rate (LVFS) levels were detected by echocardiography. Each group contained 6 rats (n = 6 per group), and all experiments were performed in triplicate. Data are expressed as mean ± standard deviation (SD). $^{\wedge\wedge}p < 0.01$, $^{\wedge\wedge\wedge}p < 0.001$ vs Blank group; $^{*}p < 0.05$, $^{**}p < 0.01$, $^{***}p < 0.001$ vs Adr group.

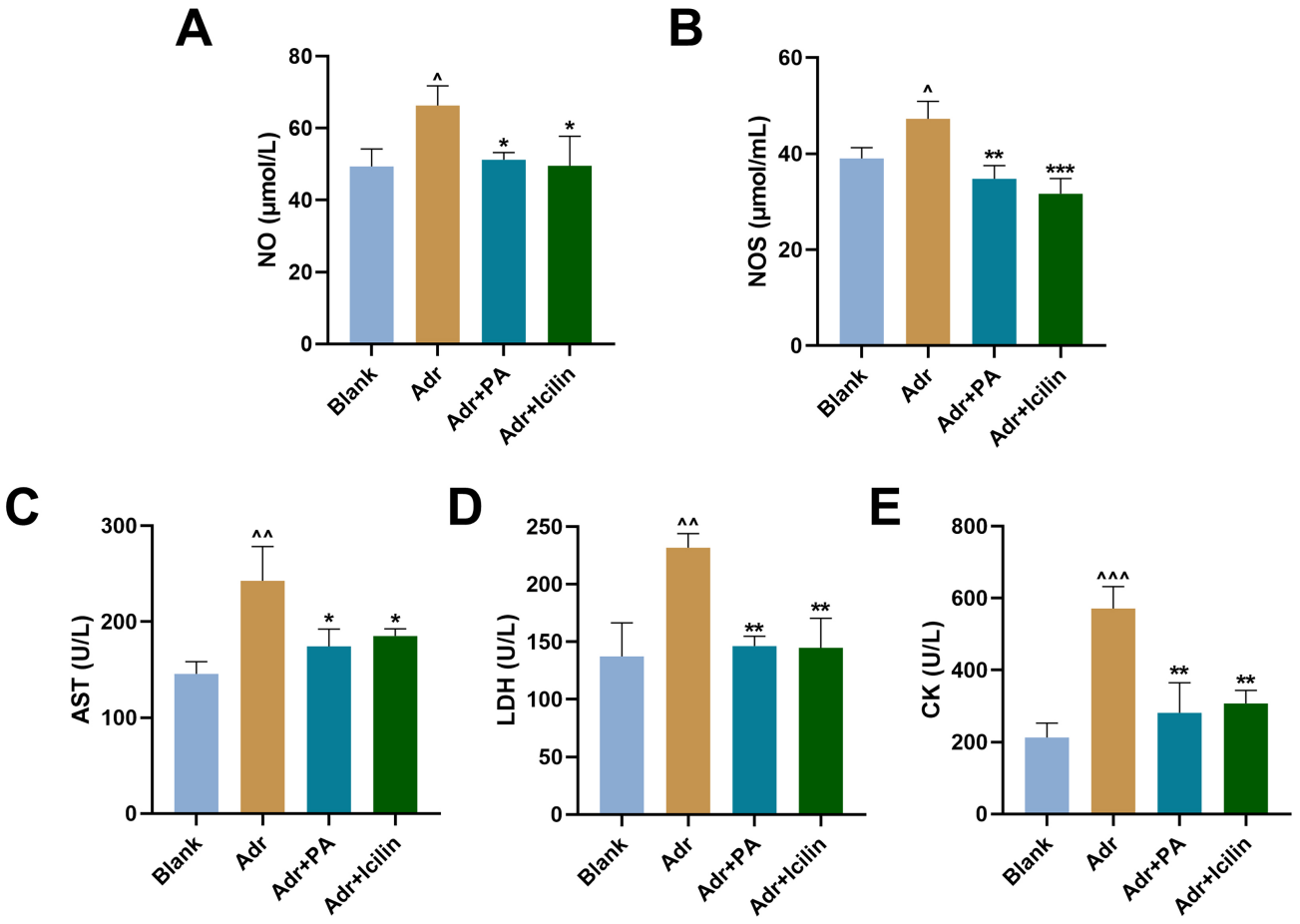

Fig. 2. PA and Icilin inhibited Adr-induced increases in NO, NOS, AST, LDH and CK levels. (A–E) The levels of nitric oxide (NO), nitric oxide synthase (NOS), aspartate aminotransferase (AST), lactate dehydrogenase (LDH) and creatine kinase (CK) in Adr-induced HF rats were detected by ELISA. Each group contained 6 rats (n = 6 per group), and all experiments were performed in triplicate. Data are expressed as mean ± SD. $^{p} < 0.05$, $^{^}p < 0.01$, $^{^^}p < 0.001$ vs Blank group; $*p < 0.05$, $**p < 0.01$, $***p < 0.001$ vs Adr group.

attenuated the Adr-induced decreases in LVEF and LVFS ($p < 0.05$). Furthermore, direct comparison between the two treatment groups revealed no significant difference in any of the above parameters, indicating that PA and Icilin have comparable cardioprotective effects in this model.

PA and Icilin Inhibited Adr-Induced Increases in NO, NOS, AST, LDH and CK Levels

NO and NOS are often used as markers of oxidative stress and inflammation in heart failure. As shown in Fig. 2A,B, Adr induced a significant upregulation of both NO and NOS levels in rat myocardial tissues, which was reversed by PA and Icilin ($p < 0.05$). To evaluate myocardial injury, serum AST, LDH, and CK levels were measured. Adr significantly increased these enzyme levels whereas PA and Icilin reversed these increases (Fig. 2C–E, $p < 0.05$). Additionally, direct comparison between PA and Icilin revealed no significant difference for any of these parameters.

PA and Icilin Alleviated Adr-Induced Myocardial Morphological Changes

H&E staining confirmed that compared with the blank group, the Adr group showed myocardial cell hypertrophy, thickened myocardial fibers, disordered cell arrangement, ruptured mitochondria, unclear cell structure, and inflammatory cell infiltration. PA and Icilin attenuated these pathological changes (Fig. 3).

PA and Icilin Counteracted Adr-Induced Regulation of Apoptosis-Related Protein Expression

Icilin is a well-established activator of the TRPM8 channel [21], and TRPM8 has been reported to reduce inflammation and cardiac remodeling after myocardial infarction [22]. Our molecular docking results also indicated that PA could bind to TRPM8. Therefore, we examined TRPM8 expression levels in the heart failure model. As shown in Fig. 4A,B, PA and Icilin significantly increased TRPM8 mRNA and protein levels in Adr-induced HF rats ($p < 0.001$), whereas Adr alone had no significant effect on TRPM8 expression.

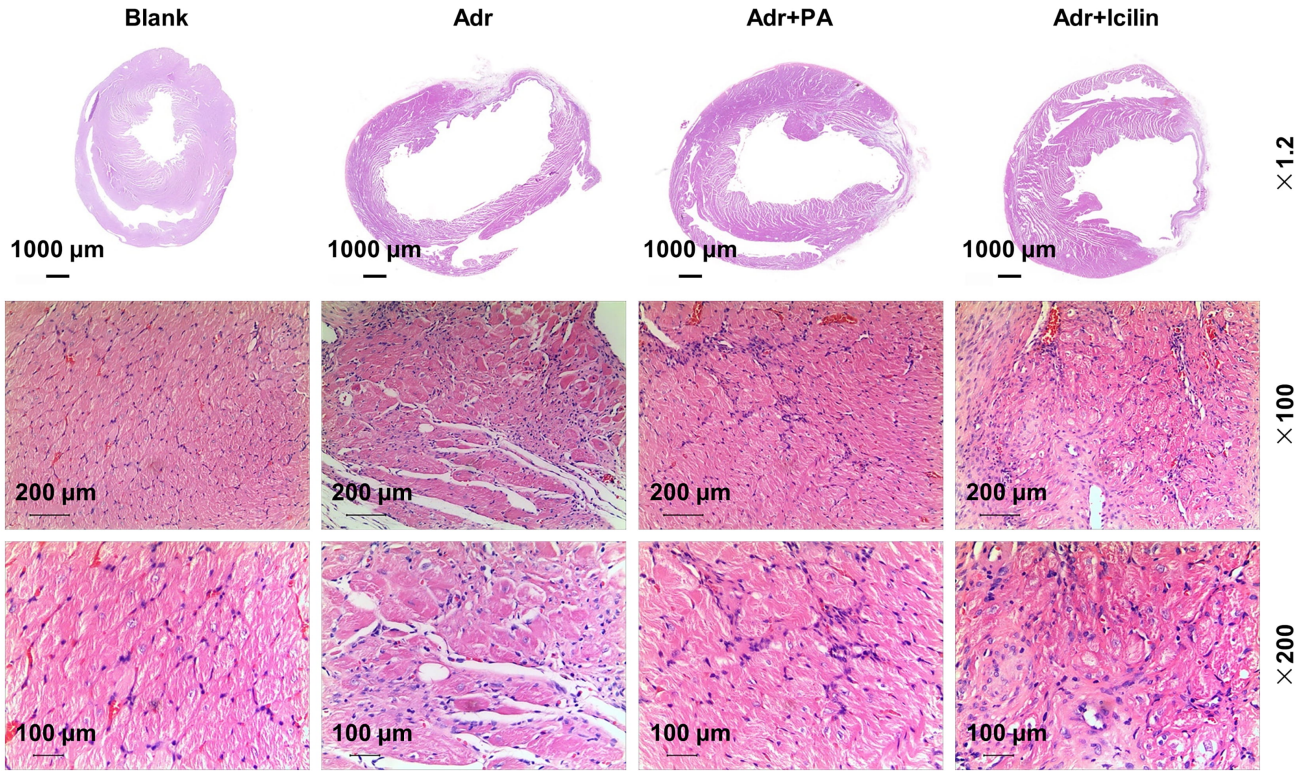

Fig. 3. PA and Icilin alleviated Adr-induced myocardial morphological changes. The effects of PA and Icilin on myocardial morphological changes in Adr-induced HF rats were detected by Hematoxylin and Eosin (H&E) staining. Each group contained 6 rats (n = 6 per group), and all experiments were performed in triplicate.

Then, we assessed apoptosis-related markers. PA and Icilin did not significantly affect the mRNA levels of caspase-3 in Adr-induced HF rats (Fig. 4C). However, PA and icilin reversed the Adr-induced downregulation of Bcl-2 mRNA and upregulation of Bax mRNA (Fig. 4C, $p < 0.05$). Consistently, Bax and cleaved caspase-3 were upregulated, whereas Bcl-2 was downregulated in Adr-induced HF rats (Fig. 4D,E, $p < 0.001$). In addition, PA and Icilin attenuated the Adr-induced increases in cleaved caspase-3 and Bax and the downregulation of Bcl-2 (Fig. 4D,E, $p < 0.05$). These results indicate that PA and Icilin partially reversed Adr-induced apoptosis. Furthermore, no significant difference was observed between PA and Icilin in their anti-apoptotic effects.

The Inhibitory Effect of PA on Apoptosis in Adr-Treated AC16 Cells Was Reversed by siTRPM8

We investigated the effects of PA and TRPM8 on apoptosis in AC16 cardiomyocytes. Western blot analysis showed that PA markedly increased TRPM8 expression in Adr-treated AC16 cells, whereas BCTC exerted the opposite effect (Fig. 5A, $p < 0.01$). Also, PA effectively attenuated Adr-induced apoptosis in AC16 cells, whereas BCTC exerted the opposite effect (Fig. 5B, $p < 0.001$). The transfection efficiency of siTRPM8 and the TRPM8 overexpression plasmid is shown in Fig. 5C; both knockdown and overexpression were successful (Fig. 5C, $p < 0.001$). TRPM8 silencing partially reversed the inhibitory effect of PA on Adr-induced apoptosis in AC16 cells (Fig. 5D, $p < 0.001$). Furthermore, TRPM8 overexpression counteracted the pro-apoptotic effect of BCTC on Adr-induced apoptosis in AC16 cells (Fig. 5E, $p < 0.001$).

Discussion

Plasma BNP level is a sensitive indicator of impaired cardiac function and can specifically reflect changes in left ventricular function in patients [23–25]. LVEF reflects the ejection capacity of the left ventricle and LVFS reflects the amplitude of ventricular contraction [26,27]. Previous studies have shown that cardiac function indicators such as NT-proBNP, BNP, LVEF, and LVFS are the most commonly utilized HF-related serum markers in clinical diagnosis and treatment, and are recommended for HF screening, diagnosis, assessment of disease severity and prognosis evaluation [28–30]. The key finding of this study is that PA effectively alleviates Adr-induced heart failure in rats. Specifically, PA treatment significantly reversed the decline in LVEF and LVFS, reduced serum BNP levels, and suppressed the expression of ANP/NPPA and BNP/NPPB in myocardial tissue. These data collectively demonstrate that PA improves cardiac function in rats with heart failure.

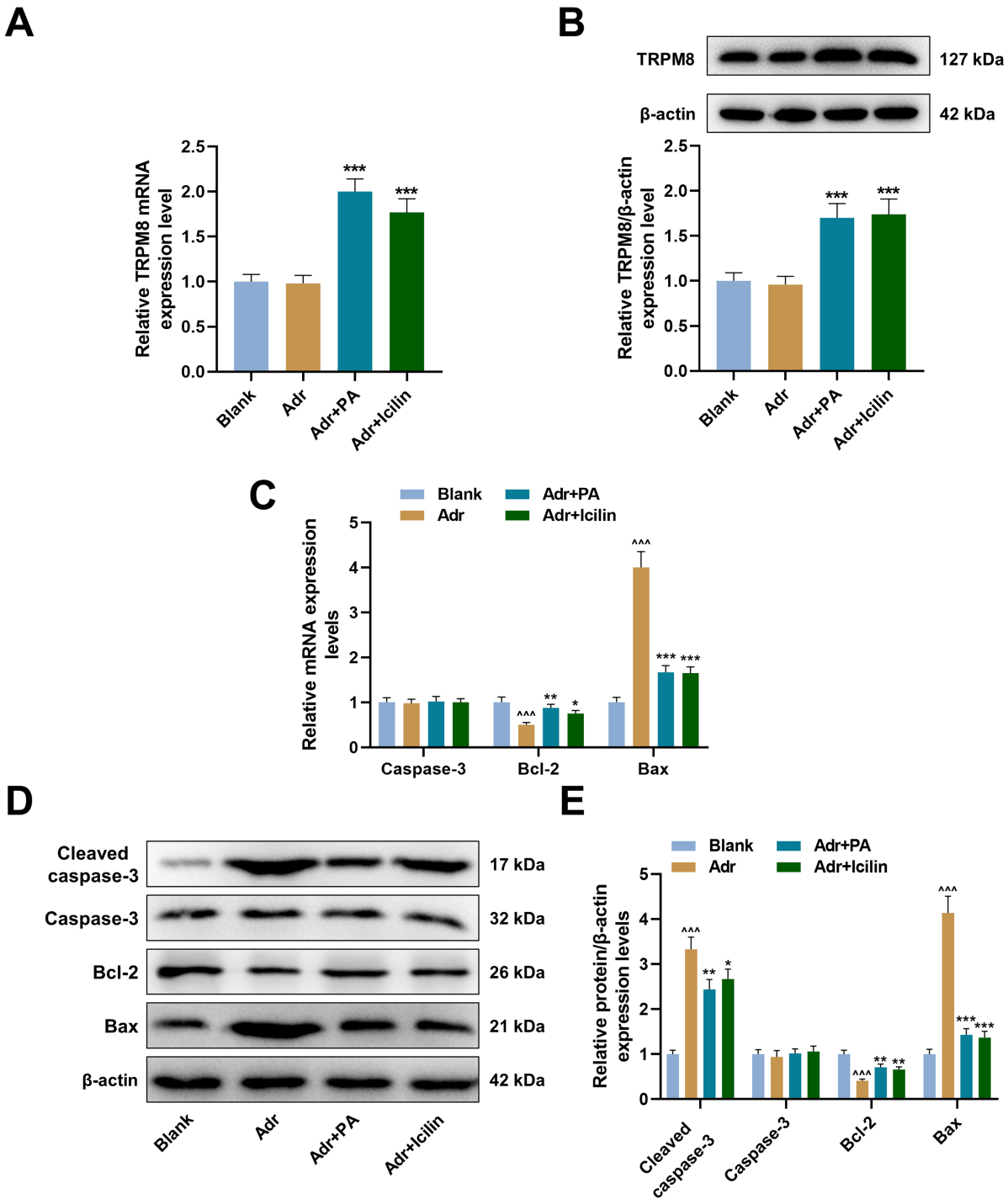

Fig. 4. PA and Icilin counteracted Adr-induced regulation of apoptosis-related protein expression. (A,B) The mRNA and protein levels of TRPM8 in Adr-induced HF rats were detected by qRT-PCR and western blot. β-actin was used as the internal control. (C–E) The apoptosis-related proteins in Adr-induced HF rats were detected by qRT-PCR and western blot. β-actin was used as the internal control. Each group contained 6 rats (n = 6 per group), and all experiments were performed in triplicate. Data are expressed as mean $\pm$ SD. $^{\wedge\wedge\wedge}p < 0.001$ vs Blank group; $^{*}p < 0.05$, $^{**}p < 0.01$, $^{***}p < 0.001$ vs Adr group.

Database analysis suggested that PA may regulate TRPM8 expression. The important role of the TRPM8 channel in the cardiovascular system has been increasingly recognized. Studies have shown that icilin (a TRPM8 agonist) can affect vascular endothelial and smooth muscle function by activating TRPM8, thereby exerting cardiovascular effects [31,32]. Moreover, TRPM8 is also closely related to metabolic disorders, myocardial hypertrophy, and heart failure [32]. Therefore, TRPM8 is considered a potential new target for treating heart failure. It should be

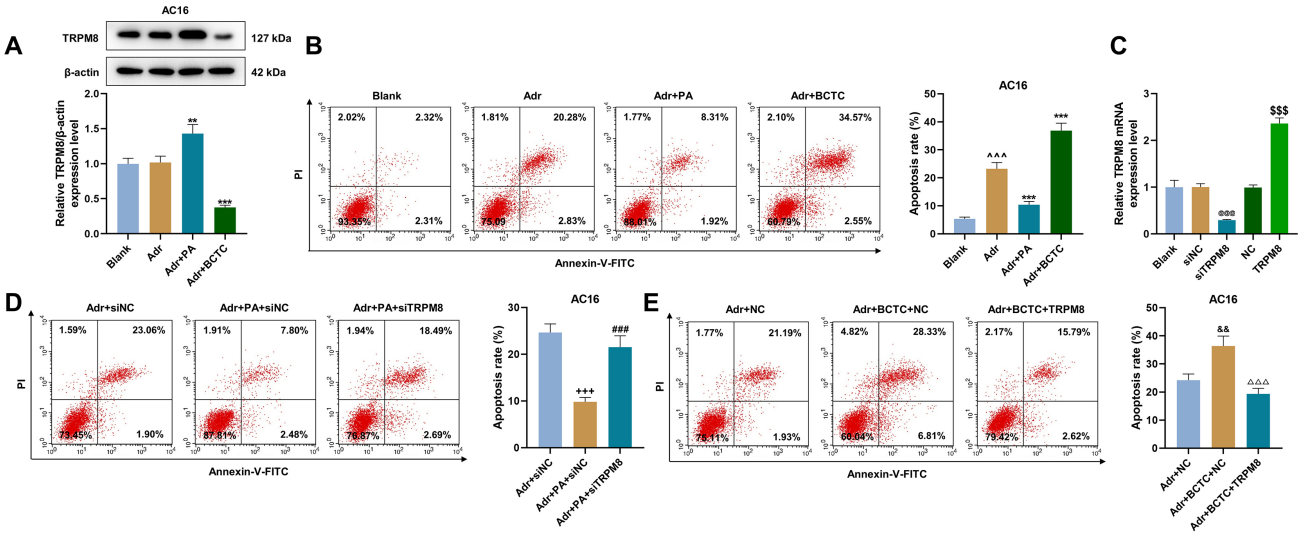

Fig. 5. The inhibitory effect of PA on apoptosis in Adr-treated AC16 cells was reversed by TRPM8 silencing. (A) The effects of PA and BCTC (a TRPM8 antagonist) on the TRPM8 expression in Adr-induced AC16 cells were assessed by western blot. β-actin was used as the internal control. (B) The effects of PA and BCTC on apoptosis in Adr-induced AC16 cells were assessed by flow cytometry. (C) The transfection efficiency of siTRPM8 and TRPM8 overexpression plasmid were detected by qRT-PCR. (D) The effects of PA and TRPM8 silencing on apoptosis in Adr-induced AC16 cells were assessed by flow cytometry. (E) The effects of BCTC and TRPM8 overexpression on apoptosis in Adr-induced AC16 cells were assessed by flow cytometry. All experiments were independently repeated three times (n = 3 biological replicates), with each experiment performed in triplicate (technical replicates). $^{**}p < 0.01$, $^{***}p < 0.001$ vs Adr group; $^{\wedge\wedge\wedge}p < 0.001$ vs Blank group; $^{@@@}p < 0.001$ vs siNC group; $^{\$\$\$}p < 0.001$ vs NC group; $^{+++}p < 0.001$ vs Adr + negative control of TRPM8 silencing (siNC) group; $^{\#\#\#}p < 0.001$ vs Adr + PA + siNC group; $^{\&\&}p < 0.01$ vs Adr + NC group; $^{\Delta\Delta\Delta}p < 0.001$ vs Adr + BCTC + NC group.

noted that icilin was used only as a positive control *in vivo* to benchmark the efficacy of PA, whereas a full range of modulators (BCTC, siRNA, and TRPM8 overexpression) was used *in vitro* to directly evaluate the necessity and sufficiency of TRPM8 in PA-mediated anti-apoptotic effects. In this study, icilin was selected as a positive control to verify the cardioprotective effects of TRPM8 pathway activation. Icilin treatment significantly reduced BNP levels and increased LVEF and LVFS in HF rats, indicating that sustained TRPM8 activation may effectively ameliorate heart failure. At the same time, our results showed that the therapeutic effect of PA was comparable to that of icilin, and no significant differences were observed for multiple indicators. These findings suggest that PA may exert cardioprotective effects through TRPM8 activation, although direct binding evidence (e.g., surface plasmon resonance) is still lacking. This further supports the hypothesis that PA may exert cardioprotective effects by regulating TRPM8. It is worth noting that there are currently no clinical studies investigating icilin or its analogues as therapies for heart failure. Icilin is valuable as a research tool because of its relative target specificity, providing a reliable reference for verifyingTRPM8 function and evaluating the efficacy of PA.

Regarding the prolonged (4-week) treatment with icilin, we acknowledge that TRPM8 agonists primarily modulate channel function. However, sustained TRPM8 activation may indirectly regulate TRPM8 expression through Ca^{2+}-dependent transcriptional feedback. Previous studies have shown that icilin stimulates TRPM8, leading to Ca^{2+} influx and subsequent activation of transcription factors such as c-Fos, Egr-1, and Elk-1 [21]. This could explain the changes in TRPM8 mRNA and protein levels observed in our study. Importantly, the Adr model did not significantly alter TRPM8 expression, indicating that the protective effect of icilin is not mediated by increasing TRPM8 levels but rather by directly activating TRPM8 channel function. Therefore, the observed upregulation of TRPM8 after prolonged treatment likely represents a secondary adaptive response to sustained channel activation rather than the primary cause of cardioprotection.

NOS isoforms produce NO, which exerts a dual, context-dependent role in the pathogenesis of HF: physiological NO derived from constitutive endothelial NOS (eNOS) mediates vascular homeostasis, anti-oxidant effects and cardioprotection, while excessive NO generated by inducible NOS (iNOS) drives nitrosative stress, inflammatory injury, and myocardial apoptosis during HF progression [33]. In Adr-induced cardiomyopathy, NO overproduction are critical mechanisms underlying myocardial oxidative damage and contractile dysfunction [34]. We also found that Adr-induced increases in NO and NOS levels in rat myocardial tissues were reversed by PA and icilin.

Moreover, we assessed the levels of HF diagnostic marker enzymes such as LDH, AST, and CK. Increased LDH and CK levels are considered specific markers of myocardial injury, whereas AST elevation is associated with various pathologies other than HF, such as liver injury and viral infection [35,36]. Measurement of serum AST, LDH and CK levels in the HF rats showed that PA and icilin significantly reduced these enzyme levels.

Cardiomyocyte apoptosis has been reported to be a key process in HF caused by various factors and is regulated by multiple apoptosis-related genes [37]. Bax is a common pro-apoptotic gene, Bcl-2 is an inhibitory gene of apoptosis and Caspase-3 is a key enzyme that causes apoptosis [38]. Their regulation of apoptosis during HF is essential to reduce HF injury [39,40]. Notably, caspase-3 is constitutively expressed as an inactive proenzyme, and its activation occurs via proteolytic cleavage rather than transcriptional upregulation. Therefore, unchanged caspase-3 mRNA levels accompanied by altered cleaved caspase-3 protein levels are biologically plausible. Cao Y *et al*. [41] have described that Adr treatment resulted in increased HF and cardiomyocyte apoptosis in C57BL/6J mice. In rats with myocardial ischemia/reperfusion (I/R) injury, BCTC, a TRPM8 antagonist, promoted apoptosis and increased Bax and cleaved caspase-3 expression, whereas icilin produced the opposite effects [32]. Thus, our study extends these previous observations by showing that PA, like icilin, exerts anti-apoptotic effects in Adr-induced HF, further supporting the involvement of the PA-TRPM8-anti-apoptotic pathway. By determining the cleaved caspase-3, Bcl-2, and Bax levels, we confirmed that PA and icilin exert an anti-apoptotic effect in Adr-induced HF rats.

To further determine whether TRPM8 mediates the effects of PA on HF, AC16 human cardiomyocytes were treated with Adr and/or PA in the presence or absence of TRPM8 silencing. TRPM8 silencing partially reversed the inhibitory effect of PA on Adr-induced apoptosis in AC16 cells, suggesting that TRPM8 activation may prevent cardiomyocyte apoptosis. Although the *in vivo* data only show a correlation between TRPM8 upregulation and reduced apoptosis, our *in vitro* loss-and gain-of-function experiments provide causal evidence that TRPM8 is necessary and sufficient for the anti-apoptotic effect of PA and icilin in cardiomyocytes.

This study investigated only the protective effects and underlying mechanism of PA in Adr-induced HF in rats and AC16 cardiomyocytes. The lack of *in vivo* validation in large animal models and clinical trials limits the direct translation of our findings to clinical practice. Furthermore, our *in vitro* validation of TRPM8 in AC16 cells using gene silencing/overexpression was limited to apoptosis assays and TRPM8 protein detection. Functional experiments were not conducted to verify the biological effects of TRPM8 on cardiomyocyte proliferation, oxidative stress, or calcium homeostasis. Additionally, we acknowledge that the conclusion that PA interacts with TRPM8 is based on molecular docking and functional consistency; definitive proof would require direct binding assays.

Conclusion

Collectively, our study demonstrates for the first time that patchouli alcohol alleviates Adr-induced HF in rats by activating TRPM8, thereby inhibiting cardiomyocyte apoptosis, ameliorating myocardial injury, and restoring cardiac function. These findings identify TRPM8 as a novel molecular target of PA in HF treatment and provide preliminary experimental evidence for natural product-based therapy against Adr-induced cardiotoxicity. Based on the current evidence, we conclude that PA may act via TRPM8 to attenuate cardiomyocyte apoptosis and HF progression, with efficacy comparable to that of the known TRPM8 agonist icilin. Future studies should include direct binding assays and exploration of downstream signaling pathways to further validate the PA-TRPM8 interaction. Follow-up studies will expand the experimental models and investigate TRPM8-mediated downstream regulatory mechanisms, as well as the clinical translational potential of PA.

Availability of Data and Materials

The analyzed datasets generated during the study are available from the corresponding author on reasonable request.

Author Contributions

SL and HC designed the research study. ZW and JY performed the research and acquisition of data. LB collected and analyzed the data. SL has been involved in drafting the manuscript and all authors have been involved in revising it critically for important intellectual content. All authors gave final approval of the version to be published. All authors have participated sufficiently in the work to take public responsibility for appropriate portions of the content and agreed to be accountable for all aspects of the work in ensuring that questions related to its accuracy or integrity.

Ethics Approval and Consent to Participate

All animal protocols were approved by the Committee of Laboratory Animals of Zhejiang Provincial Animal Center (ZJCLA-IACUC-20120022) and performed in accordance with the regulations of the China Animal Care and Use Committee. All procedures complied with the ARRIVE Guidelines 2.0.

Acknowledgment

Not applicable.

Funding

This research was supported by the Zhejiang Provincial Traditional Chinese Medicine Science and Technology Plan [grant numbers 2023ZL422] and the Zhejiang Provincial Traditional Chinese Medicine Science and Technology Plan [grant numbers 2024ZL330].

Conflict of Interest

The authors declare no conflict of interest.

References

[1] Noels H, van der Vorst EPC, Rubin S, Emmett A, Marx N, Tomaszewski M, *et al*. Renal-Cardiac Crosstalk in the Pathogenesis and Progression of Heart Failure. Circulation Research. 2025; 136: 1306–1334. https://doi.org/10.1161/CIRCRESAHA.124.325488.

[2] Yan T, Zhu S, Yin X, Xie C, Xue J, Zhu M, *et al*. Burden, Trends, and Inequalities of Heart Failure Globally, 1990 to 2019: A Secondary Analysis Based on the Global Burden of Disease 2019 Study. Journal of the American Heart Association. 2023; 12: e027852. https://doi.org/10.1161/JAHA.122.027852.

[3] Li X, Luo W, Tang Y, Wu J, Zhang J, Chen S, *et al*. Semaglutide attenuates doxorubicin-induced cardiotoxicity by ameliorating BNIP3-Mediated mitochondrial dysfunction. Redox Biology. 2024; 72: 103129. https://doi.org/10.1016/j.redox.2024.103129.

[4] Ge W, Zhang X, Lin J, Wang Y, Zhang X, Duan Y, *et al*. Rnd3 protects against doxorubicin-induced cardiotoxicity through inhibition of PANoptosis in a Rock1/Drp1/mitochondrial fission-dependent manner. Cell Death & Disease. 2025; 16: 2. https://doi.org/10.1038/s41419-024-07322-0.

[5] Yuan M, Shi H, Wang B, Cai J, Yu W, Wang W, *et al*. Targeting SOCS2 alleviates myocardial fibrosis by reducing nuclear translocation of β-catenin. Biochimica et Biophysica Acta. Molecular Cell Research. 2024; 1871: 119804. https://doi.org/10.1016/j.bbamcr.2024.119804.

[6] Cui J, Chen Y, Yang Q, Zhao P, Yang M, Wang X, *et al*. Protosappanin A Protects DOX-Induced Myocardial Injury and Cardiac Dysfunction by Targeting ACSL4/FTH1 Axis-Dependent Ferroptosis. Advanced Science. 2024; 11: e2310227. https://doi.org/10.1002/advs.202310227.

[7] Wan J, Zhang Z, Wu C, Tian S, Zang Y, Jin G, *et al*. Astragaloside IV derivative HHQ16 ameliorates infarction-induced hypertrophy and heart failure through degradation of lncRNA4012/9456. Signal Transduction and Targeted Therapy. 2023; 8: 414. https://doi.org/10.1038/s41392-023-01660-9.

[8] Cheng P, Wang X, Liu Q, Yang T, Dai E, Sha W, *et al*. LuQi formula attenuates Cardiomyocyte ferroptosis via activating Nrf2/GPX4 signaling axis in heart failure. Phytomedicine: International Journal of Phytotherapy and Phytopharmacology. 2024; 125: 155357. https://doi.org/10.1016/j.phymed.2024.155357.

[9] Hu G, Peng C, Xie X, Zhang S, Cao X. Availability, Pharmaceutics, Security, Pharmacokinetics, and Pharmacological Activities of Patchouli Alcohol. Evidence-Based Complementary and Alternative Medicine. 2017; 2017: 4850612. https://doi.org/10.1155/2017/4850612.

[10] Lee HS, Lee J, Smolensky D, Lee SH. Potential benefits of patchouli alcohol in prevention of human diseases: A mechanistic review. International Immunopharmacology. 2020; 89: 107056. https://doi.org/10.1016/j.intimp.2020.107056.

[11] Xian YF, Li YC, Ip SP, Lin ZX, Lai XP, Su ZR. Anti-inflammatory effect of patchouli alcohol isolated from Pogostemonis Herba in LPS-stimulated RAW264.7 macrophages. Experimental and Therapeutic Medicine. 2011; 2: 545–550. https://doi.org/10.3892/etm.2011.233.

[12] Xu L, Huang Q, Tan X, Zhao Q, Wu J, Liao H, *et al*. Patchouli alcohol ameliorates acute liver injury via inhibiting oxidative stress and gut-origin LPS leakage in rats. International Immunopharmacology. 2021; 98: 107897.

[13] Wang Q, Yang Y, Chen K, Li D, Tang B, Peng K, *et al*. Dietary Menthol Attenuates Inflammation and Cardiac Remodeling After Myocardial Infarction via the Transient Receptor Potential Melastatin 8. American Journal of Hypertension. 2020; 33: 223–233. https://doi.org/10.1093/ajh/hpz162.

[14] O'Connell JL, Romano MMD, Campos Pulici EC, Carvalho EEV, de Souza FR, Tanaka DM, *et al*. Short-term and long-term models of doxorubicin-induced cardiomyopathy in rats: A comparison of functional and histopathological changes. Experimental and Toxicologic Pathology. 2017; 69: 213–219. https://doi.org/10.1016/j.etp.2017.01.004.

[15] Wu Z, Zeng H, Zhang L, Pu Y, Li S, Yuan Y, *et al*. Patchouli Alcohol: a Natural Sesquiterpene Against Both Inflammation and Intestinal Barrier Damage of Ulcerative Colitis. Inflammation. 2020; 43: 1423–1435. https://doi.org/10.1007/s10753-020-01219-8.

[16] Feketa VV, Balasubramanian A, Flores CM, Player MR, Marrelli SP. Shivering and tachycardic responses to external cooling in mice are substantially suppressed by TRPV1 activation but not by TRPM8 inhibition. American Journal of Physiology. Regulatory, Integrative and Comparative Physiology. 2013; 305: R1040–R1050. https://doi.org/10.1152/ajpregu.00296.2013.

[17] Demiröz ŞM, Küçük A, Tekin E, Söylemez S, Yılmaz H, Sezen ŞC, *et al*. Cardioprotective Effects of Bosentan in Rats Subjected to Lung Ischemia-Reperfusion Injury. Medicina. 2025; 61: 1298. https://doi.org/10.3390/medicina61071298.

[18] Tan SC, Carr CA, Yeoh KK, Schofield CJ, Davies KE, Clarke K. Identification of valid housekeeping genes for quantitative RT-PCR analysis of cardiosphere-derived cells preconditioned under hypoxia or with prolyl-4-hydroxylase inhibitors. Molecular Biology Reports. 2012; 39: 4857–4867. https://doi.org/10.1007/s11033-011-1281-5.

[19] Huang F, He K. Rhizoma Zedoariae Inhibits G-CSF-Induced MDSCs-like Differentiation of THP-1 Cells. Journal of Experimental and Clinical Application of Chinese Medicine. 2024; 12–22. https://doi.org/10.62767/jecacm503.1126.

[20] Riba A, Deres L, Sumegi B, Toth K, Szabados E, Halmosi R. Cardioprotective Effect of Resveratrol in a Postinfarction Heart Failure Model. Oxidative Medicine and Cellular Longevity. 2017; 2017: 6819281. https://doi.org/10.1155/2017/6819281.

[21] Ulrich M, Wissenbach U, Thiel G. The super-cooling compound icilin stimulates c-Fos and Egr-1 expression and activity involving TRPM8 channel activation, Ca^{2+} ion influx and activation of the ternary complex factor Elk-1. Biochemical Pharmacology. 2020; 177: 113936. https://doi.org/10.1016/j.bcp.2020.113936.

[22] Alves QL, de Jesus RLC, Silva DF. Beneficial Effects Induced by TRPM8 Channels Activation to Treat Myocardial Infarction. American Journal of Hypertension. 2020; 33: 214–217. https://doi.org/10.1093/ajh/hpz195.

[23] Wu T, Xu C, Tang L, Wu X, Peng P, Yue X, *et al*. NT-pro-BNP Level is Related to Left Ventricular Remodeling in Patients With Primary Aldosteronism. Experimental and Clinical Endocrinology & Diabetes. 2024; 132: 562–569. https://doi.org/10.1055/a-2348-4468. (online ahead of print)

[24] Pan W, Zhou G, Hu M, Li G, Zhang M, Yang H, *et al*. Coenzyme Q10 mitigates macrophage mediated inflammation in heart following myocardial infarction via the NLRP3/IL1β pathway. BMC Cardiovascular Disorders. 2024; 24: 76. https://doi.org/10.1186/s12872-024-03729-x.

[25] Meng X, Zhang K, Zeng WJ, Hu ZH. Expression and Clinical Implications of pro-BNP and Soluble ST2 in Chronic Heart Failure. British Journal of Hospital Medicine. 2024; 85: 1–13. https://doi.org/10.12968/hmed.2024.0465.

[26] Robinson S, Ring L, Oxborough D, Harkness A, Bennett S, Rana B, *et al*. The assessment of left ventricular diastolic function: guidance and recommendations from the British Society of Echocardiography. Echo Research and Practice. 2024; 11: 16. https://doi.org/10.1186/s44156-024-00051-2.

[27] Zhang C, Teng X, Cao Q, Deng Y, Yang M, Wang L, *et al*. Gut microbiota dysbiosis exacerbates heart failure by the LPS-TLR4/NF-κB signalling axis: mechanistic insights and therapeutic potential of TLR4 inhibition. Journal of Translational Medicine. 2025; 23: 762. https://doi.org/10.1186/s12967-025-06821-8.

[28] Wu Y, Li T, Li P, Peng H, Gao A, Wang J, *et al*. Effects of Shenmai injection against chronic heart failure: a meta-analysis and systematic review of preclinical and clinical studies. Frontiers in Pharmacology. 2024; 14: 1338975. https://doi.org/10.3389/fphar.2023.1338975.

[29] Cheng J, Cheng T. Correlations of serum histone deacetylase 3 and thrombospondin-1 levels with cardiac function grades, ventricular remodeling, and prognosis in patients with chronic heart failure. Journal of Cardiothoracic Surgery. 2025; 20: 268. https://doi.org/10.1186/s13019-025-03467-x.

[30] McCoubrey A, Campbell RT. What is the Future of Diagnostics in Heart Failure? British Journal of Hospital Medicine. 2025; 86: 1–6. https://doi.org/10.12968/hmed.2024.0797.

[31] Silva DF, Wenceslau CF, Mccarthy CG, Szasz T, Ogbi S, Webb RC. TRPM8 channel activation triggers relaxation of pudendal artery with increased sensitivity in the hypertensive rats. Pharmacological Research. 2019; 147: 104329. https://doi.org/10.1016/j.phrs.2019.104329.

[32] Cheng QY, Yang MC, Wu J, Jia XL, Xiao C, Lian T, *et al*. Reduced cardiac ischemia/reperfusion injury by hypothermic reperfusion via activation of transient receptor potential M8 channel. Life Sciences. 2019; 232: 116658. https://doi.org/10.1016/j.lfs.2019.116658.

[33] Carnicer R, Crabtree MJ, Sivakumaran V, Casadei B, Kass DA. Nitric oxide synthases in heart failure. Antioxidants & Redox Signaling. 2013; 18: 1078–1099. https://doi.org/10.1089/ars.2012.4824.

[34] Octavia Y, Tocchetti CG, Gabrielson KL, Janssens S, Crijns HJ, Moens AL. Doxorubicin-induced cardiomyopathy: from molecular mechanisms to therapeutic strategies. Journal of Molecular and Cellular Cardiology. 2012; 52: 1213–1225. https://doi.org/10.1016/j.yjmcc.2012.03.006.

[35] Tilea I, Varga A, Serban RC. Past, Present, and Future of Blood Biomarkers for the Diagnosis of Acute Myocardial Infarction-Promises and Challenges. Diagnostics. 2021; 11: 881. https://doi.org/10.3390/diagnostics11050881.

[36] Qiu D, Cao W, Zhang Y, Hao H, Wei X, Yao L, *et al*. COVID-19 Infection, Drugs, and Liver Injury. Journal of Clinical Medicine. 2025; 14: 7228. https://doi.org/10.3390/jcm14207228.

[37] Long X, Tao S, Yang S, Li S, Rao L, Li L, *et al*. Quercetin improves heart failure by inhibiting cardiomyocyte apoptosis *via* suppressing the MAPK signaling pathway. Journal of Southern Medical University. 2025; 45: 187–196. https://doi.org/10.12122/j.issn.1673-4254.2025.01.22.

[38] Abdel-Badeea WIE, Abdel-Wahab A, Mahmoud AA, Abdel-Razik ARH, Attia EZ, Abdelmohsen UR, *et al*. Syzygium cumini Fruit Extract and Quercetin Ameliorate Cadmium-Induced Ovarian Apoptosis in Rats Via miRNA- 204 - 5p-Mediated Bcl- 2 Upregulation and Bax/Caspase 9/Caspase 3 Downregulation. Biological Trace Element Research. 2025; 203: 6172–6191. https://doi.org/10.1007/s12011-025-04632-y.

[39] Wang Q, Jiang Y, Xie S, Chen L. Exploring the Efficacy Enhancement Mechanism of Qixue Shuangbu prescription after TCM processing for treating chronic heart failure by regulating ERK/Bcl-2/Bax/Caspases-3 signaling pathway. Heliyon. 2024; 10: e30476. https://doi.org/10.1016/j.heliyon.2024.e30476.

[40] Jingxian Zhang, Xiaoping Meng. FGF19 Alleviates Cortisol-Induced Mitochondrial Damage and Apoptosis in Human Cardiomyocytes. Discovery Medicine. 2025; 3: 2224–2234. https://doi.org/10.24976/Discov.Med.202537201.189.

[41] Cao Y, Shen T, Huang X, Lin Y, Chen B, Pang J, *et al*. Astragalus polysaccharide restores autophagic flux and improves cardiomyocyte function in doxorubicin-induced cardiotoxicity. Oncotarget. 2017; 8: 4837–4848. https://doi.org/10.18632/oncotarget.13596.